# UC Davis

## UC Davis Previously Published Works


### Title

Behavior of pile foundations in laterally spreading ground during centrifuge tests


### Permalink

https://escholarship.org/uc/item/1mt502cj



### Journal

Journal of Geotechnical and Geoenvironmental Engineering, 131(11)

### ISSN

1090-0241



### Authors

Brandenberg, SJ
Boulanger, RW
Kutter, BL
et al.



### Publication Date

2005-11-01

### DOI

10.1061/(ASCE)1090-0241(2005)131:11(1378)

Peer reviewed



eScholarship.org Powered by the California Digital Library
University of California

# BEHAVIOR OF PILE FOUNDATIONS IN LATERALLY SPREADING GROUND DURING CENTRIFUGE TESTS


## PAPER NUMBER: GT/2004/023695
## HTTP://DX.DOI.ORG/10.1061/(ASCE)1090-0241(2005)131:11(1378)



**By Scott J. Brandenberg[1], Associate Member, ASCE, Ross W. Boulanger,[2] Member, ASCE, Bruce L. Kutter,[3] Member, ASCE, and Dongdong Chang[4], Student Member, ASCE**



**Abstract:** Eight dynamic model tests were performed on a 9-m-radius centrifuge to study the behavior of single piles and pile groups in liquefiable and laterally spreading ground. Pile diameters ranged from 0.36 m to 1.45 m for single piles, and from 0.73 m to 1.17 m for pile groups. The soil profile consisted of a gently sloping nonliquefied crust over liquefiable loose sand over dense sand. Each model was tested with a series of realistic earthquake motions with peak base accelerations ranging from 0.13 g to 1.00 g. Representative data that characterize the important aspects of soil-pile interaction in liquefiable ground are presented. Dynamic soil-pile and soil-pile cap forces are back calculated. Directions of lateral loading from the different soil layers are shown to depend on the mode of pile deflection relative to the soil, which depends on the deformed shape of the soil profile, the pile foundation stiffness, and the magnitude of loads imposed by the nonliquefied crust. Procedures for estimating the total horizontal loads on embedded piles and pile caps (i.e., passive loads plus friction along the base and sides) are evaluated. Due to liquefaction of the sand layer beneath the crust, the relative displacement between the pile cap and free-field crust required to mobilize the peak horizontal loads is much larger than expected based on static pile cap load tests in nonliquefied soils.



**Subject Headings:** Pile foundations; Pile groups; Pile caps; Earthquakes; Liquefaction; Centrifuge; Pile lateral loads; Soil deformation.



[1] Graduate Student, Dept. of Civil and Environ. Eng., Univ. of California, Davis, CA, 95616. email: sjbrandenberg@ucdavis.edu
[2] Professor, Dept. of Civil and Environ. Eng., Univ. of California, Davis, CA.
[3] Professor, Dept. of Civil and Environ. Eng., Univ. of California, Davis, CA.
[4] Graduate Student, Dept. of Civil and Environ. Eng., Univ. of California, Davis, CA, 95616.

## INTRODUCTION

Extensive damage to pile-supported bridges and other structures in areas of liquefaction and lateral spreading has been observed in many earthquakes around the world [e.g., Japanese Geotechnical Society (JGS) 1996, 1998]. Many important lessons and insights have been learned from case histories, physical model tests, and numerical studies in recent years, but numerous questions still remain regarding the basic mechanisms of soil-pile interaction in liquefiable soil and laterally spreading ground. Model studies can begin to clarify some of these questions, and can aid in the development of reliable design methods.

Past model tests of piles in liquefiable ground have resulted in varying observations of foundation response. Wilson et al. (1998, 2000) presented the first dynamic characterization of p-y behavior in liquefiable level ground from centrifuge model tests. Ashford and Rollins (2002) developed cyclic p-y relations from lateral load tests of piles in blast-induced liquefied soil. Tokimatsu et al. (2004) characterized p-y relations in liquefiable soil during full-scale shaking table tests. Peak subgrade reaction values in liquefiable sand were estimated from centrifuge tests by Abdoun et al. (2003) and Dobry et al. (2003). Differences in the subgrade reaction behavior observed in the above studies are consistent with the effects of relative density, pile stiffness, dynamic shaking characteristics and site response. For example, relatively small subgrade reaction loads were observed in loose sand, while larger loads were observed in medium dense sand.

A review of physical model studies and lessons from case histories showed a need for characterization of soil-pile interaction in liquefiable ground in which lateral spreading occurred. Hence, a series of dynamic centrifuge model tests were conducted on the 9-m-radius centrifuge to study the behavior of pile foundations in liquefiable and laterally spreading ground, and observations and results of the tests are presented in this paper. Single piles and pile groups were embedded in a soil profile consisting of a gently-sloping nonliquefiable crust over liquefiable loose sand over dense sand. A series of realistic earthquake motions were applied to the base of each of the models. Important quantities obtained by processing the raw recorded data, including back-calculated subgrade reaction behavior, are presented. Phasing of the subgrade reaction loads from the nonliquefied crust and liquefiable sand for different pile foundations is discussed, and factors that influence the different observations are explained. Theoretical predictions of the lateral loads imposed on the pile foundation by the laterally spreading crust (including passive loads on the upslope face, and friction between the crust and the sides and base of the cap) are compared

with measured ultimate loads ($F_{crust,ult}$). Finally, the relative displacements between the free-field soil and the pile cap required to mobilize the ultimate loads are compared with those for static pile cap load tests in nonliquefied soil profiles, and a load transfer relationship representing soil-pile cap interaction for a crust overlying liquefiable sand is presented.

## CENTRIFUGE TESTS

Eight dynamic centrifuge tests were performed on the 9-m radius centrifuge at the Center for Geotechnical Modeling at the University of California, Davis. Models were tested in a flexible shear beam container (FSB2) at centrifugal accelerations ranging from 36.2g to 57.2g. Results are presented in prototype units.

### Soil Properties

Fig. 1 shows schematic model layouts for the first centrifuge test PDS01 and for test SJB03, which is similar to all seven of the tests after PDS01. The soil properties for four of the tests are summarized in Table 1. The soil profile for all of the models consisted of a nonliquefiable crust overlying loose sand ($D_r \approx$ 21-35%) overlying dense sand ($D_r \approx$ 69-83%). All of the layers sloped gently toward a river channel carved in the crust at one end of the model. The nonliquefiable crust consisted of reconstituted Bay mud (liquid limit ≈ 88, plasticity index ≈ 48) that was mechanically consolidated with a large hydraulic press, and subsequently carved to the desired slope. The sand layers beneath the crust consisted of uniformly-graded Nevada Sand ($C_u$ = 1.5, $D_{50}$ = 0.15 mm). A thin layer of coarse Monterey sand was placed on the surface of the Bay mud for some of the models. Water was used as a pore fluid for all of the models.

The undrained shear strength of the clay, $s_u$, for each test was measured using a T-bar (Stewart and Randolph, 1991). The $s_u$ profile from the T-bar tests was reasonably consistent with the $s_u$ profile estimated using a normalized strength ratio (e.g. Ladd and Foott, 1974) according to:

$$s_u = 0.25 \cdot \sigma_{vc}' \cdot \left(\frac{\sigma_{vp}'}{\sigma_{vc}'}\right)^{0.8} \quad (1)$$

where $\sigma_{vc}'$ = the vertical effective consolidation stress, and $\sigma_{vp}'$ = the maximum vertical effective consolidation stress applied to the clay during model preparation. Average $s_u$ values for the clay layers are reported in Table 1. The T-bar tests were conducted at a strain rate that was about an order of magnitude smaller than occurs during

shaking on the centrifuge, so the $s_u$ values have been increased by 10% to account for rate effects (e.g. Ladd and Foott, 1974; Sheahan et al., 1996).

**Foundation Properties**

The properties of the pile foundations used in each test are provided in Table 1. The first test, PDS01, contained three single piles of various diameters and a two-pile group with an above ground pile cap that provided fixed-head conditions. Subsequent tests included a six-pile group with a large pile cap embedded in the nonliquefied crust. The pile caps for the six-pile groups provided a stiff rotational restraint at the connection between the pile and the cap with the measured rotational stiffness being about 1,300,000 kN·m/rad for the tests at 57.2 g and 390,000 kN·m/rad for the tests at 38.1 g. The last two tests contained superstructures with different natural periods.

**Simulated Earthquakes**

Each test was shaken with a number of simulated earthquakes conducted in series with sufficient time between shakes to allow dissipation of excess pore pressures. The simulated earthquakes were scaled versions of the acceleration recordings either from Port Island (83-m depth, north-south direction) during the Kobe earthquake, or from the University of California, Santa Cruz (UCSC/Lick Lab, Channel 1) during the Loma Prieta earthquake. These earthquake motions were chosen because they contain different frequency content and shaking characteristics. Generally, the shake sequence applied to the models was a small event ($a_{max,base}$ = 0.13g to 0.17g) followed by a medium event ($a_{max,base}$ = 0.30g to 0.45g) followed by one or more large events ($a_{max,base}$ = 0.67g to 1.00g).

The sequence of shaking events likely induced changes in the soil properties, including densification of the sand layers due to post-shaking consolidation, and cyclic degradation of the stress-strain behavior in the clay. Volumetric strains that were measured during excavation of the models after all of the shaking events indicated that the change in relative density of the dense sand layer was negligible and that the increase in relative density of the loose sand layer was roughly 10% on average. However, the change in relative density is likely to be non-uniform throughout the layer. The progressive increase in relative density and the accumulation of prior shaking history is expected to cause a progressive increase in liquefaction resistance of the sand during the series of shaking events. Nonetheless, the repeated large shaking events were sufficiently strong to induce liquefaction throughout the loose sand layer in

spite of prior densification, which is similar to the common observation that liquefaction of natural sand deposits re-occurs during different earthquakes.

### Data Archives

Complete data reports from the centrifuge tests are presented by Singh et al. (2000a,b, 2001), and Brandenberg et al. (2001a,b, 2003). Conventions for naming the Test ID in this paper are the same as those in the data reports. The data are available on the Center for Geotechnical Modeling website (http://nees.ucdavis.edu). A small portion of the data is presented in this paper.

## MEASUREMENTS AND DATA PROCESSING

Some forces and displacements were not directly measured, but rather were obtained by processing the raw recorded data. This section presents the data processing techniques that were used to obtain subgrade reaction behavior, pile displacement, soil displacement, and loads imposed on the pile caps by the soil.

### Subgrade Reaction Behavior

The soil-pile subgrade reaction, p, can be calculated from the recorded moment distribution along the pile using beam theory according to the equation

$$p(z) = \frac{d^2}{dz^2} M(z) \tag{2}$$

where M is the moment, and z is depth along the pile. Numerical differentiation can be very sensitive to relatively small errors in the moment data, particularly near the pile head and tip, and at locations where the distribution of p varies sharply. The data processing scheme and method of differentiation are therefore critical for obtaining accurate p-histories. In this study the data processing methods and the weighted residual numerical differentiation procedure developed by Wilson et al. (2000) were used.

### Pile Displacement

The displacement of the piles, $y_{pile}$, can be calculated from measured boundary conditions and the recorded curvature distribution along the pile using the equation

$$\frac{d^2}{dz^2} y_{pile}(z) = \phi(z) \tag{3}$$

where $\phi$ is curvature. For linear elastic material behavior, $M = EI\phi$. Integrating to solve for $y_{pile}$ requires specification of two boundary conditions. The measured pile head displacement relative to the container base was used for one of the boundary conditions, and the pile tip displacement relative to the container base was assumed to be zero for the other. The measured pile head rotation provided an independent check on the reasonableness of the computed shape. The calculated pile displacement profiles contained contributions from curvature along the piles and rotation at the pile tips.

**Soil Displacement**

The free-field soil displacement, $y_{soil}$, ranged from relatively high-frequency dynamic movement to relatively low-frequency permanent displacement. Horizontal displacement transducers attached to the clay crust by vertical anchor plates provided the low frequency part of the crust displacement, but the high frequency component was inaccurate due to transient rotation of the anchor plates during shaking. The dynamic component of the soil displacement was calculated by double integration of acceleration records, but the permanent displacement could not be obtained in this way because double integration is sensitive to very small noise levels in the low-frequency portion of the signals containing the permanent displacement data. The crust displacement was therefore calculated by adding together the low frequency component from the displacement transducers and the high frequency component from the double-integrated accelerations. The permanent component of the deeper sand displacements was not measured by transducers, but was estimated based on measurements of the soil deformation profile taken when the model was dissected after all of the shaking events. All displacement values were calculated relative to the base.

**Relative Displacement Between Piles and Soil**

The subgrade reaction is related to the relative displacement between the piles and the soil ($y = y_{pile} - y_{soil}$). The calculated time histories of y were difficult to accurately determine because they contained measurement errors that were attributed primarily to assumptions regarding the boundary conditions required to calculate $y_{pile}$ and the low frequency part of $y_{soil}$. The results do, however, permit qualitative observations of the relative displacement profiles

at snapshots in time. Hence, time histories are presented for p, but not for y, while snapshots of the displaced shapes of the soil and piles are presented for critical loading cycles.

**Lateral Loads on Pile Caps**

Strain gauges oriented in Wheatstone full bridges to measure shear (hereafter called shear gauges) located on the piles near the interface between the loose sand and clay provided a measure of the shear forces, $V_s$, $V_n$ and $V_c$, as shown in the free-body diagram in Fig. 2. These shear forces had contributions from loads imposed on the foundation by the clay crust and from pile cap inertia. The loading imposed on the pile group by the crust, $F_{crust}$, was calculated as the difference between the total shear and the cap inertia force.

$$F_{crust} = \left(2 \cdot V_s + 2 \cdot V_n + 2 \cdot V_c\right) + a_h \cdot m_{cap} \tag{4}$$

where the cap inertia force is $-a_h \cdot m_{cap}$. A simple superstructure attached to the pile caps for some of the tests contributed an additional inertia component that was also subtracted out to obtain $F_{crust}$ for those tests. The pile cap acceleration was measured for every test except PDS03 and the cap inertia was therefore estimated for PDS03, as described later.

The calculated crust load includes the passive resistance on the upslope face of the pile cap, friction on the sides and base of the cap, and loads on the pile segments between the shear gauges and the bottom of the cap as shown in Fig. 2.

$$F_{crust} = F_p + F_2 + F_4 + 2 \cdot F_s + 2 \cdot F_c + 2 \cdot F_n \tag{5}$$

These components of horizontal soil loading could not be calculated separately based on the test data, therefore estimates of the various components were made analytically as described later in the paper. Active loading on the down-slope face of the cap was excluded from the free-body diagram because large gaps formed along this face when the soil spread laterally down-slope, and are believed to have remained open during the large earthquake motions. However, during the small earthquake motions, the gap was small and may have closed during upslope displacement cycles.

The lateral loading mechanism in Fig. 2 assumes that the clay beneath the pile cap flows around the piles, thereby mobilizing lateral loads on the pile segments and friction loads at any contact between the crust and the base

of the cap. However, there is another possible mechanism in which the clay crust beneath the pile caps becomes trapped between the piles, thereby acting as an equivalent block. In such cases, the passive force and side friction forces would act along the entire thickness of the nonliquefied crust layer, while the lateral loads on the pile segments and base of the pile cap would be considered internal forces (i.e. not external to a free body of the equivalent block). The controlling mechanism is that which produces the smaller total lateral load. The pile groups in the centrifuge tests all exhibited the failure mechanism in Fig. 2 in which the clay crust flowed around the pile segments, which was verified both by photos taken after the tests during excavation of the models and by comparison of theoretical predictions of the total lateral loads for each mechanism.

**Accuracy of Numerical Differentiation**

The shear gauges on the piles provide a means of verifying the accuracy of the shear- and p- histories obtained from differentiation of the moment distributions. Fig. 3 shows two shear (V) histories, one measured directly by the shear gauges and the other from differentiation of the moment distributions ($V = dM/dz$). The two time histories exhibit similar dynamic characteristics, similar peak loads, and both show non-zero initial offsets that represent residual loads remaining from previous earthquakes. The reasonable agreement between the time histories indicates that the data processing methods and differentiation technique are sufficient to produce reasonably accurate first derivatives of moment with depth. Most of the p-histories are believed to be accurate with the exception of zones near soil layer interfaces or the pile head or tip, though an independent check of the accuracy of the p-histories ($p = d^2M/dz^2$) could not be obtained from the measured data.

## OBSERVATIONS FROM SJB03

Observations from centrifuge test SJB03 are presented in detail in this section and comparisons with other centrifuge tests are made in later sections. A series of four simulated earthquake events were applied to model SJB03. The first was a small Santa Cruz motion with a peak acceleration of 0.13g. Soil deformation, excess pore pressure ratio, pile cap displacement and moments were all relatively small during the small Santa Cruz motion, as summarized in Table 2. The subsequent motions were a medium Santa Cruz ($a_{max,base} = 0.35g$), a large Santa Cruz ($a_{max,base} = 0.67g$) and a large Kobe ($a_{max,base} = 0.67g$). The loading mechanics are most clearly illustrated during the large motions, so observations will be presented in reverse chronological order beginning with the large Kobe motion, then the large Santa Cruz motion, and finally the medium Santa Cruz motion .

**Large Kobe Motion**

Several time histories of raw and processed data illustrate the behavior of the soil and the pile group during the large Kobe motion in Fig. 4. The bending moment 2.7 m below the ground surface was the recording from the moment bridge on the southeast pile (denoted SEM for South East pile with bending Moment bridges) that was closest to the pile cap connection, where the peak moments were measured during the test. The time histories of p and $r_u$ were near the middle of the loose sand layer, and $r_u$ was in the free-field (about 13 m down-slope of the pile group). The sign conventions for bending moment, pile cap inertia, subgrade reaction and displacement are shown in Fig. 2. The displacement of the clay crust was measured at a location between the side face of the cap and the wall of the model container, and was probably influenced by the walls of the container and the pile cap. A truly "free-field" crust displacement could not be obtained during the tests because the pile group influenced the crust displacements throughout the model, but the crust displacement was measured at a location where these influences are small, and will be treated as "free-field" in this paper.

At the time that the peak bending moment was measured during the large Kobe motion (8840 kN·m), the following also occurred:

- The lateral load from the clay crust was 5730 kN, which was the maximum for the large Kobe motion.
- The pile cap inertia force was 5790 kN, which was the maximum for the test.
- The subgrade reaction, p, 6.7 m below the ground surface was –370 kN/m, which was a local minimum. Note that the subgrade reaction was negative; the loose sand restrained the pile from moving down-slope.
- The excess pore pressure ratio was 0.5, near a local minimum, in spite of having been close to 1.0 earlier in the motion, and returning to near 1.0 later in the motion.
- The displacement of the pile cap was 0.5 m, and was approaching a local maximum that was larger than the permanent pile cap displacement of about 0.3 m at the end of shaking.
- The displacement of the clay crust was 2.3 m, which was less than the permanent crust displacement of nearly 3.5 m.

The relative displacement between the crust and the pile cap was 3.2 m by the end of the large Kobe motion, which was sufficient to develop passive pressure against the upslope face of the pile cap.

Several transient drops in pore pressure in the loose sand during shaking are attributed to undrained shear loading of dilatant soil. Dilatancy is defined as the tendency of sand to dilate during drained shear loading. Dilatancy results in an increase in effective stress (decrease in pore pressure) during undrained shear loading. The transient drops in pore pressure are attributed to dilatancy rather than to drainage because the rate of post-shaking pore pressure dissipation shows that drainage is far too slow to affect pore pressures during the short duration of an individual cycle of shaking.

**Large Santa Cruz Motion**

The large Santa Cruz motion and large Kobe motion had the same peak base acceleration amplitude ($a_{max,base}$ = 0.67g) and the dynamic responses exhibited some similar trends that can be seen by comparing Figs. 4 and 5. At the time that the peak bending moment occurred during the large Santa Cruz motion (7080 kN·m), the following also occurred:

- The peak lateral load from the clay crust was 6380 kN, which was the maximum for all events.
- The subgrade reaction in the loose sand was near a local minimum of -310 kN/m, and the loose sand restrained down-slope movement of the piles.
- The excess pore pressure ratio was near a transient minimum of 0.7.
- The displacement of the pile cap was 0.3 m, which was close to the residual pile cap displacement after shaking.
- The displacement of the clay crust was 1.3 m, which was less than the residual crust displacement of 1.8 m after strong shaking.

The relative displacement between the crust and the pile cap was 1.5 m after shaking, which was large enough to mobilize passive resistance on the upslope face of the pile cap. The lateral load from the clay crust (see Table 2) was slightly larger during the large Santa Cruz motion than for the large Kobe motion that followed, which indicates that the passive pressures were mobilized during the Santa Cruz motion, and subsequent total lateral loads decreased slightly due to a progressive loss of contact between the crust and the sides and base of the pile cap, and to progressive cyclic degradation of the stress-strain behavior of the clay during successive earthquakes. Note,

however, that the pile cap inertia was significantly larger for the Kobe motion than for the large Santa Cruz, hence the total lateral forces exerted on the cap were largest for the Kobe motion.

The different shaking characteristics between the large Kobe and Santa Cruz motions resulted in some differences in the pile group response. The pile cap inertia force was 2560 kN at the time of peak bending moment during the large Santa Cruz motion, which was about 60% of the peak for the shake, and less than 50% of the peak from the Kobe motion. The peak bending moment was 7080 kN·m, which is only 80% of the peak moment from the Kobe motion. The smaller peak bending moment was likely caused by the smaller pile cap inertia for the large Santa Cruz motion. The dips in $r_u$ due to dilatancy were smaller, and the loads imposed on the piles by the loose sand were smaller during the large Santa Cruz motion than during the Kobe motion. Given that the peak base acceleration amplitudes for the large Santa Cruz and large Kobe motions were the same, the differences in the responses indicate that peak acceleration is insufficient to characterize the response of the pile groups, and that the frequency content of the motion is also important.

**Medium Santa Cruz Motion**

The medium Santa Cruz motion with $a_{max,base}$ = 0.35g was smaller than the two large motions, and produced a peak $r_u$ value of about 0.7. In spite of such important differences as the smaller $r_u$, the following trends observed for large motions (Figs. 4 and 5) were also true of the medium Santa Cruz motion (Fig. 6) at the time of peak bending moment:

- The lateral load from the clay crust reached its maximum for the event (2870 kN).
- The subgrade reaction was near a transient minimum of -150 kN/m, and the loose sand restrained down-slope movement of the piles.
- The excess pore pressure ratio was near a transient minimum of 0.5 due to dilatancy.

The displacement of the clay crust was about 0.35 m at the end of shaking, while the displacement of the pile cap was only about 0.03 m. The rather large relative displacement of 0.32 m would generally be considered sufficient to mobilize the passive resistance of the clay crust against the upslope face of the pile cap based on experience with static load tests of pile groups in nonliquefied soil profiles. However, the peak crust load for the medium Santa Cruz motion was only 2870 kN, which is less than 50% of the peak load observed during the large

shakes. The load transfer behavior observed in the centrifuge test was significantly softer than that observed in nonliquefied ground, and is discussed in more detail later in the paper.

**Timing of Lateral Loads from the Liquefiable Layer and Nonliquefiable Crust**

The peak bending moment for each event always coincided with the peak down-slope loading from the clay crust for that event. At that instant, the liquefiable sand layer provided a resisting force, contrary to the common expectation that the load acts in the same direction as the soil displacement (JRA 2002; Dobry et al. 2003). This observation can be explained by considering the timing of the down-slope crust displacement, the lateral load from the clay crust, and the phase transformation behavior of the liquefiable sand. Each time the crust began a down-slope displacement cycle the lateral load from the clay crust progressively increased, and after some straining in the loose sand, its free-field $r_u$ dropped due to dilatancy (i.e., as during cyclic mobility behavior). The relatively large lateral load from the crust caused incremental down-slope displacements of the piles in the loose sand layer. The temporarily stiffened loose sand layer moved down-slope less than the piles during the cycle, resulting in an upslope resisting load from the liquefiable sand. Furthermore, the magnitude of the soil-pile interaction force is larger than commonly associated with liquefiable soil because the sand was temporarily stiffer and stronger due to the transient drop in $r_u$.

The above mechanisms are further illustrated by the snapshots of soil displacement, pile displacement, bending moment, p, and $r_u$ shown in Fig. 7 for the Kobe motion at the time of peak bending moment and at the time of peak pile cap displacement. At the time of peak bending moment, $r_u$ values were low across nearly the entire depth of the loose sand layer in spite of high values earlier and later in the shake. Some of the peaks in $r_u$ reported in Fig. 7 are larger than 1.0, which may be due to transducer movements or changes in total stress caused, for example, by transient stress waves or the movement of the clay crust layer. The $r_u$ values were highest near the interface between the clay and the sand, likely due to pore water becoming trapped beneath the low-permeability crust layer. The trapping of pore water beneath the clay can cause the loose sand layer to become looser in a zone near the top of the loose sand due to void redistribution (Kulasingam et al., 2004), thereby enabling the clay crust to slide on top of the loose sand. The resulting large displacement discontinuity allowed development of passive pressure of the crust against the pile cap with relatively small soil displacement in the loose sand layer. The temporarily stiffened loose

sand layer resisted nearly the entire lateral crust load (as illustrated by the moment and p profiles in Fig. 7), with only small loads mobilized against the portion of the piles in the dense sand.

**Timing of Lateral Loads at the Time of Peak Pile Cap Displacement**

The directions of loads acting on the foundation at the time of peak pile cap displacement were similar to those observed at the time of peak bending moment, but the magnitudes were different (Fig. 7). Figs. 4 and 5 show that the peak cap displacement occurred about ¼ loading cycle after the peak bending moment for the large shakes. During this ¼ loading cycle $r_u$ increased as the loose sand began an unloading cycle, the piles moved down-slope slightly, and the peak positive bending moment shifted downward below the interface between the loose and dense sand (Fig. 7). The large resisting force provided by the transiently dilating loose sand became a smaller resisting force during the ¼ cycle as the loose sand experienced unloading, and the dense sand near the loose/dense interface provided the largest resisting force. The peak pile cap displacement was associated with a softening in the load-displacement response of the foundation, and not with the largest imposed loading.

## RESULTS FROM OTHER CENTRIFUGE TESTS

**Timing of Lateral Loads from Spreading Crust and Cap Inertia**

The lateral loads imposed on the pile caps by the clay crust and by pile cap inertia are shown in Fig. 8 for tests SJB01 and SJB03 during the large Kobe motion. The cap acceleration was not measured for test PDS03, so the total shear imposed on the pile cap during the large Kobe motion is plotted instead. The highest loads from the laterally spreading clay crust were mobilized during transient peaks in each test, and were not maintained at the end of shaking. A number of large loading cycles occurred during each event, and the residual end-of-shaking crust loads on the pile caps were less than 60% of the peak loads during each event. The crust loads were highest for SJB03, which can be attributed primarily to the larger pile cap compared with the other two tests (Table 1). The crust loads were smaller for PDS03 than for SJB01, which can be attributed to the lower undrained shear strength of the crust in PDS03 (Table 1). Analytical predictions of lateral loads on pile caps are presented later.

The pile cap inertia for SJB01 was small compared with the crust load imposed on the cap, and the loads were generally not in-phase during critical loading cycles. In contrast, the magnitude of the pile cap inertia was significant for SJB03 and acted in-phase with the crust loads during all of the large loading cycles. While the

conditions that influence the phasing of pile cap inertia and lateral crust load are not yet clearly understood, the closer phasing during SJB03 may be due to the larger pile foundation (Table 1) being laterally stiffer than the pile foundation in SJB01.

**Timing of Lateral Loads from Liquefiable Layer and Nonliquefiable Crust**

The relative timing of lateral loads from the liquefiable layer and the nonliquefiable crust during the peak loading cycles for the single piles from PDS01 were sometimes consistent with those observed for the six-pile groups, but sometimes inconsistent. The subgrade reaction behavior for the 0.73-meter diameter single pile (denoted MP for Medium Pile) and the 0.73-m-diameter two-pile group (denoted GN for 2-pile Group, North pile) in PDS01 exhibited the same trends as six-pile groups (i.e., piles mobilized upslope resisting forces in the liquefiable sand during the critical loading cycles). In contrast the 1.45-m-diameter single pile (denoted BP for Big Pile) attracted down-slope loads from the liquefiable sand during the critical loading cycles.

The behavior of BP during a large Kobe motion ($a_{max,base}$ = 0.78g) is summarized in several representative time series shown in Fig. 9. The critical loading cycles (peak moment, peak displacement) for BP occurred during down-slope crust displacement, and during phase transformation in the loose sand layer. The peak bending moment occurred early during shaking when the down-slope load from the clay crust peaked (e.g. as represented by p at 2.4 m depth) and the loose sand developed a local minimum in $r_u$ due to dilatancy. However, in contrast to observations for SJB03 (Figs. 4-6), the loose sand imposed a small down-slope loading on the pile at the time of peak bending moment. A second peak moment later in shaking also coincided with a transient drop in $r_u$ in the loose sand, and a larger down-slope load between the pile and liquefiable sand. An important distinction is that the loose sand imposed down-slope loads on BP (Fig. 9) during critical loading cycles, but provided upslope resisting loads during the critical loading cycles for the six-pile groups (Figs. 4-6).

Fig. 10 shows p-histories near the middle of the loose sand during large Kobe motions for the 0.73-m-diameter single pile (MP), the 0.73-m-diameter upslope pile from the two-pile group (GN), and the 1.45-m-diameter pile (BP) from PDS01, and for the southeast, upslope 1.17-m diameter pile (SEM) from SJB03. The peak crust load, incremental peak down-slope displacements of the piles, incremental peak ground surface displacement and p in the liquefiable sand at the time of peak moment are shown in Table 3 for the foundations in PDS01 during the first large Kobe motion. At the time that the peak bending moment occurred in each of the piles, BP (largest-diameter pile)

attracted a down-slope load from the liquefiable sand, GN (two-pile group) attracted a moderate upslope resisting load, MP (more flexible pile) mobilized a larger upslope resisting load, and SEM mobilized the largest upslope resisting load.

The direction of loading in the liquefied sand can be explained by the relative displacements between the piles and the liquefiable sand layer during the critical loading cycles. Fig. 11 schematically demonstrates three different loading cases that were observed during the centrifuge tests. For case A, the pile is stiff enough to resist the loads imposed by the crust while displacing less than the liquefied sand layer. Hence, the pile attracts a down-slope load from the liquefied sand, similar to BP. For case B, the foundation is stiff enough to resist the load from the clay crust, but the pile displaces more than the liquefied sand layer and attracts an upslope resisting load from the liquefied sand, similar to piles MP, GN and SEM. For case C, the pile is too flexible and/or weak to mobilize the full down-slope passive pressure of the nonliquefied crust layer. In such cases, the pile head displacement is larger than the ground surface displacement because the crust layer provides a gripping action on the pile. This type of behavior was observed for the small-diameter pile SP in test PDS01 (Boulanger et al., 2003), and also for flexible pile foundations presented by Abdoun et al. (2003) and Dobry et al. (2003). Variations in free-field soil displacement among centrifuge models and at different locations within a single model caused some differences in the responses of the different piles, but the stiffness of the piles relative to the soil profile is believed to be the primary factor controlling the direction of relative displacement between the piles and free-field soil, and hence the direction of loading from the liquefiable sand layer.

Lateral loads from liquefied soil are often represented in static seismic design methodologies as relatively small down-slope pressures. For example, JRA (2002) suggests down-slope pressures equal to 30% of the total overburden stress, which corresponds to p of 18-40 kN/m for the 0.73-1.45 m diameter piles in Fig. 10, respectively. Dobry et al. (2003) suggest that down-slope pressures in the liquefiable sand can be neglected when a nonliquefiable crust spreads on top of the liquefiable layer. These design recommendations are significantly different from of the values observed in the centrifuge tests, both in loading magnitude and direction. It is unlikely, however, that static seismic design methods can be used to accurately model the complicated dynamic phasing and subgrade reaction behavior in the liquefied sand. Alternatively, the simpler guidelines for representing liquefied soil may be recognized as crude static representations of more complex dynamic loading conditions, with subsequent efforts being made toward quantifying the uncertainty that such approximations introduce into the computed responses of a pile foundation.

## CALCULATED VERSUS RECORDED LATERAL CRUST LOADS

Theoretical methods for calculating the lateral loads imposed on the pile foundation by the lateral spreading clay crust were evaluated against the recorded ultimate values. The recorded lateral loads on the pile foundations were measured using shear gauges on the piles a short distance beneath the bottom of the pile cap. Hence, the peak measured lateral loads include pile cap inertia, the passive force on the upslope pile cap face, the friction forces on the sides and base of the pile cap, and the lateral forces on the pile segments between the pile cap base and the shear gauges (Fig. 2). For comparison purposes the results are presented in terms of the peak lateral crust loads imposed on the pile group (i.e. the peak crust load on the pile cap is the measured load in the shear gauges minus the inertia forces of the pile cap and any superstructure).

### Passive Earth Pressure on Pile Cap

The peak passive load imposed on the upslope face of each pile cap was estimated using a Coulomb-based analysis. The nonliquefied crust some tests consisted of Monterey sand overlying clay, so the Coulomb method was modified to account for soil layering as shown in Fig. 12. For the surface Monterey sand layer, the passive force, $F_{p,sand}$, and the force on the failure wedge, R, were assumed to be the same as for a pile cap with height $H_{sand}$ in a uniform sand layer. For SJB03 the layer thicknesses were $H_{sand}$ = 0.8 m and $H_{clay}$ = 1.4 m (Fig. 12). The properties for the clay are in Table 1, and properties for the Monterey sand were estimated to be $\gamma$ = 17 kN/m$^3$, $\phi'$ = 36$^o$, $\delta$ = 22$^o$, and $c'$ = 0. The remaining forces in Fig. 12 are solved from force equilibrium. The inertia of the soil failure wedge was also included as Okabe (1926) and Mononobe and Matsuo (1929) originally proposed for cohesionless soils. The inertial coefficient $k_h$ (Fig. 12) was taken as 0.2 for all tests, and changes in $k_h$ made only small differences in the estimated crust loads (increasing $k_h$ to 0.6 amounted to less than a 10% increase in crust load for SJB03). The influence of $k_h$ on the predicted crust load was presented by Boulanger et al. (2003).

### Lateral Friction Forces on the Pile Caps

The friction forces between the clay and the sides of the pile caps ($F_{2clay}$) were calculated using $F_{2clay} = \alpha\, s_u\, A_{sides1}$, where $\alpha$ is the adhesion coefficient and $A_{sides1}$ was the contact area between the clay and the pile cap. Adhesion coefficients were taken as the median values from the plot of $\alpha$ vs. $s_u$ (Terzaghi et al., 1996). The friction forces between the Monterey sand and the sides of the pile caps ($F_{2sand}$) were calculated using

$F_{2sand} = ½ \gamma K_o H_1 \tan(\delta) A_{sides2}$ where $K_o$, the coefficient of earth pressure at rest, was taken as $1-\sin(\phi')$, $A_{sides2}$ is the contact area between the Monterey sand and the pile cap. The friction force on the base of the pile cap was calculated as $F_4 = \alpha R_{base} s_u A_{base}$, where $A_{base}$ is the area of the base of the pile cap minus the area of the piles, and $R_{base}$ is a reduction factor to account for (1) the decrease in contact area as the crust settled away from the base of the cap, and (2) the decrease in base friction stress due to interaction between the lateral stresses on the piles beneath the cap and the friction stress on the base of the cap.

**Lateral Forces on Piles**

The peak lateral loads applied to piles by the laterally spreading clay crust were calculated using the bearing equations by Matlock (1970):

$$p_u = N_p \cdot s_u \cdot b \tag{6}$$

$$N_p = \left( 3 + \frac{\sigma_v'}{c} + J \frac{z}{b} \right) \qquad \text{for } z \le z_{cr} \tag{7}$$

$$N_p = 9 \qquad \text{for } z > z_{cr} \tag{8}$$

where $N_p$ is the bearing factor, J is an empirical constant, assumed to be 0.5 in this study, and z is depth below the ground surface. Eq. 7 controls at shallow depths, and is based on a wedge-type failure mechanism in which the failure mass exhibits vertical deformation, while Eq. 8 is based on a plane-strain solution in which the clay flows around the pile without vertical deformation.

Matlock (1970) found that displacement-controlled cyclic loading of piles in clay reduced the p-y resistance compared to that for static monotonic loading. The p-y curves for cyclic loading had a peak resistance that was 72% of the ultimate resistance for static loading, followed by further reductions in resistance that depended on the depth and magnitude of y. These "cyclic loading" p-y curves were derived for loading conditions that are more representative of wave or wind loading, whereas the loading conditions encountered during lateral spreading are very different. Matlock's "cyclic loading" p-y curves substantially under-estimate the peak lateral loads imposed by a laterally spreading crust (Boulanger et al. 2003), as will be illustrated later for the single piles in PDS01.

Matlock's bearing equations were developed for single piles in clay with a free ground surface such that a failure wedge on the passive side of the pile could exhibit some upward vertical displacement at shallow depths. If a gap exists between the base of a pile cap and the underlying clay, then failure wedges against the piles can move upwards. In this case, the depth z in Matlock's equations would be best taken as relative to the base of the pile cap. If the base of a pile cap is in contact with the underlying clay, then the clay may be restrained to fail in plain strain against the piles, producing larger bearing factors [i.e. Eq. (8) versus (7)] Back-calculated values for the peak subgrade reaction loads on the pile segments at mid-depth in the clay beneath the pile cap for SJB03 at the time of peak moment (Fig. 7) ranged from about 200 kN/m to about 450 kN/m, which corresponds to quite reasonable bearing factors of $N_p = 3.9$ to $N_p = 8.7$, respectively. The accuracy of these back-calculated values is limited by the small number of strain gauges in the clay layer beneath the cap, and so the comparison with Matlock's bearing equations really only represents a qualitative check on the consistency of the data. Consequently, in the absence of a suitable equation for bearing factors on piles beneath pile caps, the loads on the pile segments beneath the caps were estimated using Matlock's equations with the depth z being relative to the adjacent ground surface, which gives $N_p$ values intermediate to those calculated for plane strain and for a gap beneath the cap.

**Total Lateral Crust Loads on Pile caps**

The total lateral load on the pile cap was calculated for each test, and $R_{base}$ was adjusted so the predictions agreed reasonably with the measured ultimate crust loads. The total loads and the individual components estimated from the analysis are presented in Table 4. The passive force exerted on the upslope face of the pile cap ranged from 43% to 50% of the total crust load, with pile segment forces and side and base friction accounting for the remaining fraction. Neglecting friction forces in design would result in a substantial under-prediction of the peak loads that were measured during the test, which would be unconservative. The base friction reduction factor, $R_{base}$, ranged from 0 to 1/2, with an average value of 1/4. The range in $R_{base}$ is consistent with observations of the contact between the crust and base of the pile cap during model excavation, with more gaps being observed for the tests with low back-calculated $R_{base}$ values.

**Total Lateral Crust Loads on Single Piles**

The peak measured p-values against piles BP and GN near the center of the clay layer are summarized in Table 5, along with static $p_{ult}$ values predicted using Matlock's bearing factors. This comparison of measured and

calculated $p_{ult}$ values is made for the center of the clay where the differentiation of the recorded bending moment distribution is most accurate (i.e. away from interfaces and boundaries). Values are not compared for MP because electronic drift in bending moment recordings in the crust layer induced errors in the second derivatives in the crust. The predicted values are close to the measured peak values, which indicate that Matlock's static bearing factors are appropriate to use for piles in laterally spreading clays at shallow depths. The p-values predicted using Matlock's (1970) cyclic loading p-y curves are less than 25% of the static $p_{ult}$ values (Table 5), and would have resulted in a significant under-prediction of pile displacements and bending moments for these tests.

**Crust Load versus Relative Displacement between Free-Field Soil and Pile Cap**

The centrifuge test data provide a means of assessing the load transfer relation for a laterally spreading crust over liquefiable soil. Fig. 13 shows crust load vs. relative displacement at virgin loading peaks (i.e. crust load peaks that exceed the maximum past crust load) from tests with a six-pile group. The recorded loads were normalized by the ultimate load measured for each test. Relative displacement, which was the soil displacement to the side of the pile cap minus the pile cap displacement, was normalized by pile cap height. The largest loads were mobilized at relative displacements of 40% to over 100% of the pile cap height, which is much larger than commonly observed for static pile cap load tests.

For static loading of retaining walls, the magnitude of wall displacement required to mobilize passive resistance is generally considered to be about 0.5 % to 5 % of the wall height depending on soil type and density. Static load tests on a pile group in granular soil by Rollins and Sparks (2002) indicate that the peak load was mobilized at a pile cap displacement of about 2.5% to 6% of the pile cap height. Duncan and Mokwa performed load tests on bulkheads and pile groups embedded in natural desiccated sandy silt and sandy clay, and in crusher run gravel and sand backfills (Duncan and Mokwa 2001; Mokwa and Duncan 2001). Ultimate loads for their tests were developed at displacements of about 1% of the pile cap height for the natural soil and 4% for the backfill soils.

The softer load-displacement response observed in the centrifuge tests compared with static load tests can be attributed in part to cyclic degradation of the clay stress-strain response caused by the previous loading cycles. The load-displacement response in the centrifuge tests would likely have been stiffer if one large displacement cycle occurred instead of a series of progressively increasing loading cycles. However, the differences between the static load tests and the centrifuge tests are too large to be explained by cyclic degradation alone.

The primary cause of the softer load-displacement response of the crust loads on the pile caps was the influence of the underlying liquefied soil on the distribution of stresses in the nonliquefied crust. For a hypothetical case where the underlying sand is not liquefied, some of the stress imposed on the clay by the pile cap would geometrically spread down into the sand, and shear stress in the clay crust would decrease sharply with distance away from the pile cap. For the case where the underlying sand is liquefied (with greatly reduced strength and stiffness), little of the stress imposed on the clay by the pile cap would be spread down into the liquefied sand, and thus the lateral stress in the clay crust would decrease more slowly with distance away from the pile cap. The spreading of lateral stress to greater distance away from the pile cap causes larger strains in the clay that is outside of the eventual failure wedge. Since the relative displacement between the pile cap and the free-field soil is an integral of strains between two reference points, the result is a much softer load versus relative displacement response for the crust over liquefied soil than for a crust supported on nonliquefied soil. The load transfer mechanism is discussed in more detail by Brandenberg et al. (2004).

Several trend lines are also shown in Fig. 13, and were developed according to Eq. 9.

$$\frac{F_{crust}}{F_{crust,ult}} = \left[ \left( \frac{y}{C \cdot H} \right)^{-0.33} + \left( \frac{16 \cdot y}{C \cdot H} \right)^{-1} \right]^{-1} \leq 1 \qquad (9)$$

where $F_{crust}$ is the load on the pile cap, $F_{crust,ult}$ is the ultimate load, y is the relative displacement between the free-field crust and the pile cap, H is the height of the pile cap, and C is an empirical curve-fitting constant that controls the stiffness of the curve. The relationship can be visualized as consisting of an elastic and a plastic component in series. The case for no liquefaction is most closely associated with C = 0.04, for which passive resistance is mobilized at about 5% of the pile cap height. The curve with C = 0.4 produces the best fit with the data, and is associated with the passive resistance being mobilized at about 50% of the pile cap height. Further experimental and analytical studies are needed however, to determine how the observed load transfer relation should be adjusted for the range of conditions encountered in practice (i.e. other cap dimensions and soil stratigraphies).

## SUMMARY AND CONCLUSIONS

Centrifuge models with single piles and pile groups that penetrated a sloping profile with a nonliquefied crust overlying a liquefiable sand layer, overlying a dense sand layer were shaken with a series of realistic earthquake

motions. In these experiments, significant strains developed in the liquefiable sand, and the laterally-spreading crust displaced more than the liquefiable sand. Effects of crust strength, pile diameter and pile cap dimensions on lateral load behavior were studied. Back-calculation of time series of lateral loads on the piles and pile caps provided new insight regarding the mechanisms that affect the magnitude and direction of the lateral loads from the crust and from the liquefiable layer. The direction of lateral loads was shown to depend on the direction of the incremental and total relative movements between the soil and piles.

Regarding the loads on piles from the laterally spreading clay crust, the peak lateral loads were predicted well by Matlock's (1970) "static" p-y curves, whereas his "cyclic loading" p-y curves were very unconservative. The peak loading produced by down-slope spreading of the clay crust is more closely approximated by a static monotonic loading mechanism than by the displacement-controlled cyclic loading used in Matlock's studies.

Regarding the loads on the pile caps from the clay crust, the side and base friction between the embedded pile caps and the crust were found to contribute significantly to the total crust loads exerted on the pile foundations. Base friction, often ignored by designers because of the impression that clay will settle away from the pile cap, can be significant if the crust comes in contact with the bottom of the cap as lateral spreading causes the clay to wedge between the pile cap and the underlying soil layers. Large relative displacements were required to mobilize peak crust loads when the soil beneath the crust liquefied because a large length of the crust (uphill of the pile cap) was compressed before pressures were sufficient to cause passive failure. The mechanism is different from that of a retaining wall or pile cap in the absence of liquefaction.

Regarding the loads from the liquefiable soil on the piles, a variety of displacement patterns in the soil layers and piles were identified. For piles that were stiff relative to the surrounding soil (e.g. Case A in Fig. 2), the liquefiable soil tended to push the piles down-slope along with the crust. For more flexible piles, the liquefiable soil sometimes produced large upslope forces on the pile when the crust pulled the pile down-slope such that the down-slope movement of the pile was greater than that of the liquefiable soil. These loading patterns are more complex than those that are often assumed in static seismic analysis procedures (e.g., JRA, 2002; Dobry et al., 2003). Designers should recognize that such analysis procedures use crude approximations to envelope the critical loading patterns that occur under more complex dynamic loading conditions, and should use caution in extrapolating analytical models beyond the ranges of their experimental validation.

## ACKNOWLEDGMENTS

Funding was provided by Caltrans under contract numbers 59A0162 and 59A0392 and by the Pacific Earthquake Engineering Research (PEER) Center, through the Earthquake Engineering Research Centers Program of the National Science Foundation, under contract 2312001. The contents of this paper do not necessarily represent a policy of either agency or endorsement by the state or federal government. The centrifuge shaker was designed and constructed with support from the National Science Foundation (NSF), Obayashi Corp., Caltrans and the University of California. Recent upgrades have been funded by NSF award CMS-0086566 through the George E. Brown, Jr. Network for Earthquake Engineering Simulation (NEES). Center for Geotechnical Modeling (CGM) facility manager Dan Wilson, and CGM staff Tom Kohnke, Tom Coker and Chad Justice provided assistance with centrifuge modeling. Former UC Davis graduate student Priyanshu Singh oversaw some of the centrifuge tests, and performed some data processing.

## APPENDIX. REFERENCES

Abdoun, T., Dobry, R., O'Rourke, T.D., and Goh, S.H. (2003). "Pile Response to Lateral Spreads: Centrifuge Modeling." *J. Geotech. Geoenviron. Eng.*, ASCE, Vol. 129(10), 869-878.

Ashford, S. A., and Rollins, K. M. (2002). *TILT: The Treasure Island Liquefaction Test: Final Report*, Report SSRP-2001/17, Department of Structural Engineering, University of California, San Diego.

Brandenberg, S. J., Singh, P., Boulanger, R. W., and Kutter, B. L. [2001 (a)]. "Behavior of piles in laterally spreading ground during earthquakes – centrifuge data report for SJB01." Report No. UCD/CGMDR-01/02, Center for Geotechnical Modeling, Department of Civil Engineering, University of California, Davis.

Brandenberg, S. J., Singh, P., Boulanger, R. W., and Kutter, B. L. [2001 (b)]. "Behavior of piles in laterally spreading ground during earthquakes – centrifuge data report for SJB02." Report No. UCD/CGMDR-01/06, Center for Geotechnical Modeling, Department of Civil Engineering, University of California, Davis.

Brandenberg, S. J., Chang, D., Boulanger, R. W., and Kutter, B. L. (2003). "Behavior of piles in laterally spreading ground during earthquakes – centrifuge data report for SJB03." Report No. UCD/CGMDR-03/03, Center for Geotechnical Modeling, Department of Civil Engineering, University of California, Davis.

Brandenberg, S.J., Boulanger, R.W., Kutter, B.L., Wilson, D.W., and Chang, D. (2004). "Load transfer between pile groups and laterally spreading ground during earthquakes." *13th World Conference on Earthquake Engineering*, Vancouver, Canada, paper No. 1516.

Boulanger, R. W., Kutter, B. L., Brandenberg, S. J., Singh, P., and Chang, D. (2003). Pile foundations in liquefied and laterally spreading ground during earthquakes: Centrifuge experiments and analyses. Report UCD/CGM-03/01, Center for Geotechnical Modeling, Univ. of California, Davis, CA.

Dobry, R., Abdoun, T., O'Rourke, T. D., and Goh, S. H. (2003). "Single Piles in Lateral Spreads: Field Bending Moment Evaluation." *J. Geotech. Geoenviron. Eng.*, ASCE, Vol. 129(10), 879-889.

Duncan, M.J., and Mokwa, R.L. (2001). "Passive Earth Pressures: Theories and Tests." *J. Geotech. Geoenviron. Eng.*, ASCE, Vol. 127(3), 248-257.

Japanese Geotechnical Society (1996). Special Issue on Geotechnical Aspects of the January 17, 1995, Hyogoken-Nambu Earthquake, Soils and Foundations, Tokyo.

Japanese Geotechnical Society (1998). Special Issue No. 2 on Geotechnical Aspects of the January 17, 1995, Hyogoken-Nambu Earthquake, Soils and Foundations, Tokyo.

JRA (2002). *Specifications for highway bridges*. Japan Road Association, Preliminary English Version, prepared by Public Works Research Institute (PWRI) and Civil Engineering Research Laboratory (CRL), Japan, November.

Kulasingam, R., Malvick, E.J., Boulanger, R.W., and Kutter, B.L. (2004). "Strength Loss and Localization at Silt Interlayers in Slopes of Liquefied Sand." *J. Geotech. Geoenviron. Eng.*, ASCE, Vol. 130(11), 1192-1202.

Ladd, C.C., and Foott, R. (1974). "New Design Procedure for Stability of Soft Clays." *J. of Geotech. Eng. Division*, ASCE, Vol. 100(GT7), 769-786.

Matlock, H. (1970). "Correlations of design of laterally loaded piles in soft clay." *Proc. Offshore Technology Conference*, Houston, TX, Vol 1(1024), 577-594.

Mokwa, R.L., and Duncan, M.J. (2001). "Experimental Evaluation of Lateral-Load Resistance of Pile Caps." *J. Geotech. Geoenviron. Eng.*, ASCE, Vol. 127(2), 185-192.

Mononobe, N. and Matsuo, H. (1929). "On the determination of earth pressures during earthquakes." *Proceedings, World Engineering Congress, 9 p.*

Okabe, S. (1926). "General theory of earth pressures." *Journal of the Japan Society of Civil Engineering*, Vol. 12(1).

Rollins, K. M., and Sparks, A. (2002). "Lateral resistance of full-scale pile cap with gravel backfill." *J. Geotech. Geoenviron. Eng.*, ASCE, Vol. 128(9), 711-723.

Sheahan, T.C., Ladd, C., and Germaine, J.T. (1996). "Rate-Dependent Undrained Shear Behavior of Saturated Clay." *J. Geotech. Geoenviron. Eng.*, ASCE, Vol. 122(2), 99-108.

Singh, P., Subramanian, P. K., Boulanger, R. W., and Kutter, B. L. [2000 (a)]. "Piles under earthquake loading – centrifuge data report for PDS01." Report No. UCD/CGMDR-00/05, Center for Geotechnical Modeling, Department of Civil Engineering, University of California, Davis.

Singh, P., Boulanger, R. W., and Kutter, B. L. [2000 (b)]. "Piles under earthquake loading – centrifuge data report for PDS02." Report No. UCD/CGMDR-00/06, Center for Geotechnical Modeling, Department of Civil Engineering, University of California, Davis.

Singh, P., Brandenberg, S. J., Boulanger, R. W., and Kutter, B. L. (2001). "Piles under earthquake loading – centrifuge data report for PDS03." Report No. UCD/CGMDR-01/01, Center for Geotechnical Modeling, Department of Civil Engineering, University of California, Davis.

Stewart, D.P. and Randolph, M.F. (1991). "A New Site Investigation Tool for the Centrifuge," Proc., Centrifuge ′91, H.-Y. Ko and F. G. McLean, eds., Balkema, Rotterdam, 531-538.

Terzaghi, K., Peck, R. B., and Mesri, G. (1996). *Soil Mechanics in Engineering Practice.* 3rd ed. New York, John Wiley and Sons, 549 pp.

Tokimatsu, K., Suzuki, H., and Sato, M. (2004). "Effects of inertial and kinematic forces on pile stresses in large shaking table tests." *13th World Conference on Earthquake Engineering*, Vancouver, Canada, paper No. 1322.

Wilson, D.W., Boulanger, R.W., and Kutter, B.L. (1998). "Signal processing for and analysis of dynamic soil-pile-interaction experiments." Proc., Centrifuge '98, Kimura, Kusakabe, and Tamura, eds., Balkema, Rotterdam, 1:135-140.

Wilson, D. W., Boulanger, R. W., and Kutter, B. L. (2000). “Seismic lateral resistance of liquefying sand.” *J. Geotech. Geoenviron. Eng.*, ASCE, Vol. 126(10), 898-906.

**Figure 1: Centrifuge model layouts with most of the approximately 100 transducers per model omitted for clarity.**

**Figure 2: Free-body diagram of the pile cap and pile segments above the shear gauges.**

**Figure 3: Comparison of a shear force time series obtained from the shear gauges and from differentiating the bending moment distribution on pile SEM during a large Kobe motion for test SJB03.**

**Figure 4: Representative time series from SJB03 for the large Kobe motion.**

**Figure 5: Representative time series from SJB03 for the large Santa Cruz motion.**

**Figure 6: Representative time series from SJB03 for the medium Santa Cruz motion.**

**Figure 7: Snapshots of displacement, moment, p and $r_u$ at the time of peak moment and at the time of peak pile cap displacement from SJB03 for the large Kobe motion.**

**Figure 8: Time series of the lateral crust loads imposed on the six-pile groups from PDS03, SJB01 and SJB03.**

**Figure 9: Representative time series from PDS01 for the large-diameter single pile, BP, for the large Kobe motion.**

**Figure 10: p-histories near the middle of the loose sand for MP, GN and BP from PDS01 and SEM from SJB03 during a large Kobe motion.**

**Figure 11: Schematic of soil and pile displacements for cases where piles could not resist the downslope passive force from the crust (C) and cases where the piles resisted the passive force of the crust with either upslope resisting forces from the loose sand (B) or downslope driving forces from the loose sand (A).**

**Figure 12: Free-body diagram for a two-layer Coulomb-based passive force analysis.**

**Figure 13: Normalized load vs. normalized relative displacement from centrifuge tests and various trend lines calculated using Eq. (9).**

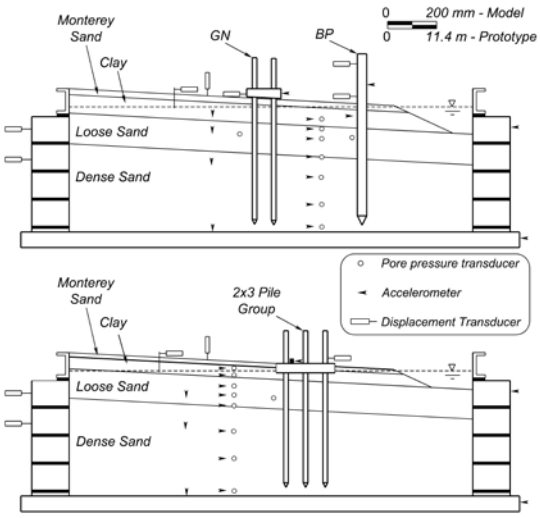


**Figure 1: Centrifuge model layouts with most of the approximately 100 transducers per model omitted for clarity.**

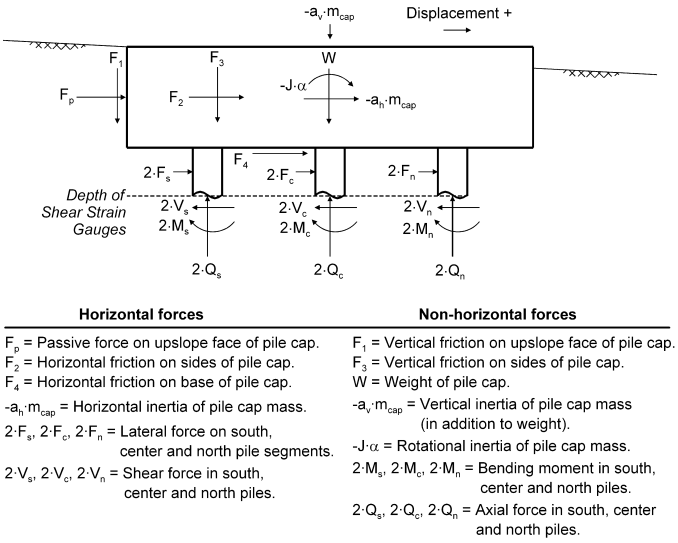


**Horizontal forces**

$F_p$ = Passive force on upslope face of pile cap.
$F_2$ = Horizontal friction on sides of pile cap.
$F_4$ = Horizontal friction on base of pile cap.
$-a_h \cdot m_{cap}$ = Horizontal inertia of pile cap mass.
$2 \cdot F_s$, $2 \cdot F_c$, $2 \cdot F_n$ = Lateral force on south, center and north pile segments.
$2 \cdot V_s$, $2 \cdot V_c$, $2 \cdot V_n$ = Shear force in south, center and north piles.

**Non-horizontal forces**

$F_1$ = Vertical friction on upslope face of pile cap.
$F_3$ = Vertical friction on sides of pile cap.
W = Weight of pile cap.
$-a_v \cdot m_{cap}$ = Vertical inertia of pile cap mass (in addition to weight).
$-J \cdot \alpha$ = Rotational inertia of pile cap mass.
$2 \cdot M_s$, $2 \cdot M_c$, $2 \cdot M_n$ = Bending moment in south, center and north piles.
$2 \cdot Q_s$, $2 \cdot Q_c$, $2 \cdot Q_n$ = Axial force in south, center and north piles.

**Figure 2: Free-body diagram of the pile cap and pile segments above the shear gauges.**

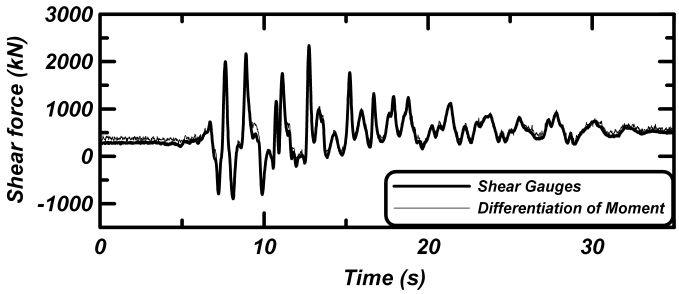


**Figure 3: Comparison of a shear force time series obtained from the shear gauges and from differentiating the bending moment distribution on pile SEM during a large Kobe motion for test SJB03.**

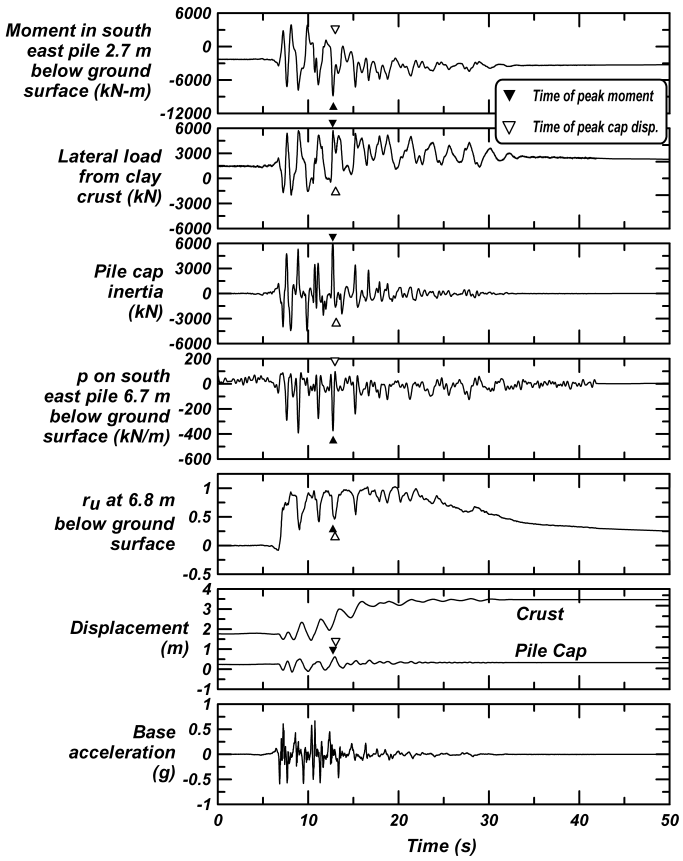


**Figure 4: Representative time series from SJB03 for the large Kobe motion.**

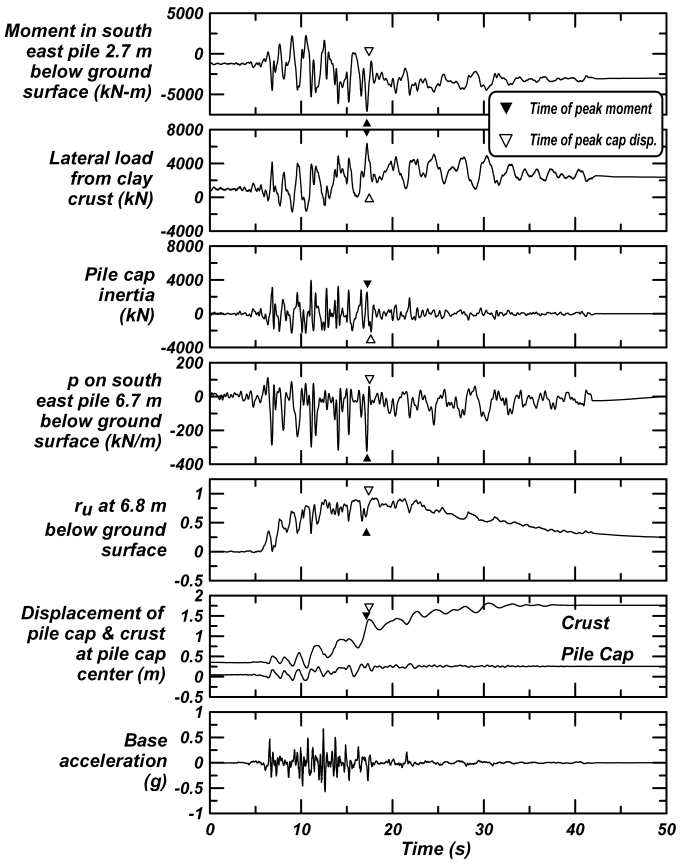


**Figure 5: Representative time series from SJB03 for the large Santa Cruz motion.**

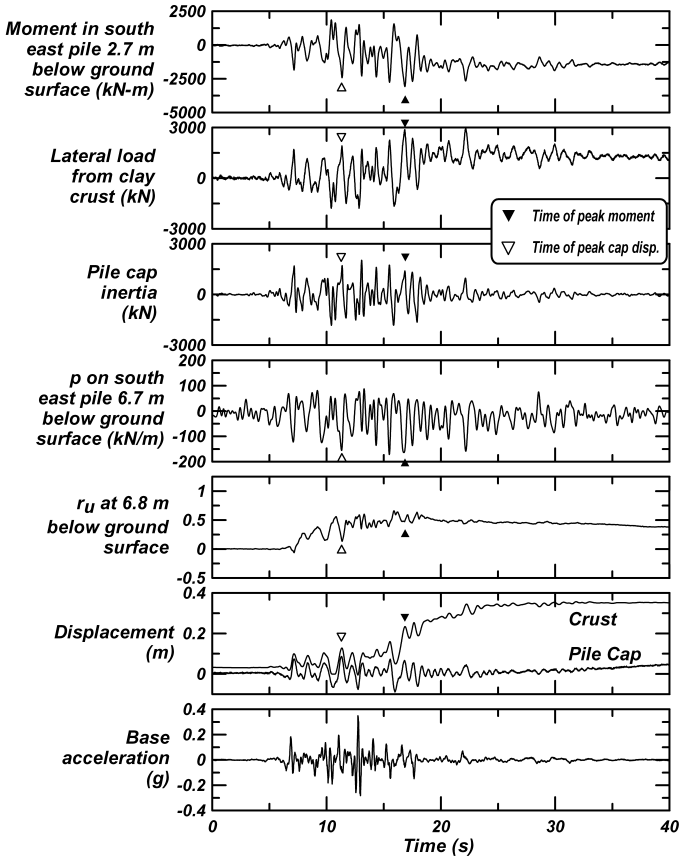


**Figure 6: Representative time series from SJB03 for the medium Santa Cruz motion.**

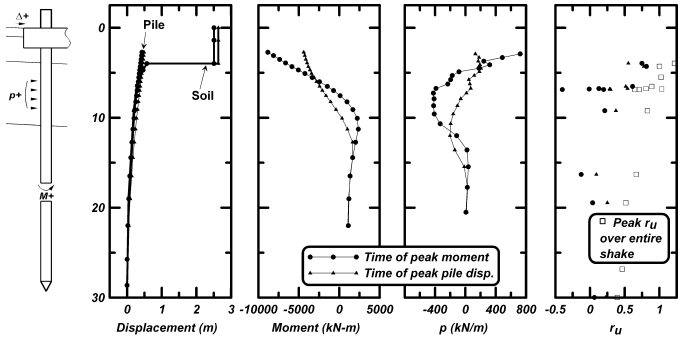


**Figure 7: Snapshots of displacement, moment, p and $r_u$ at the time of peak moment and at the time of peak pile cap displacement from SJB03 for the large Kobe motion.**

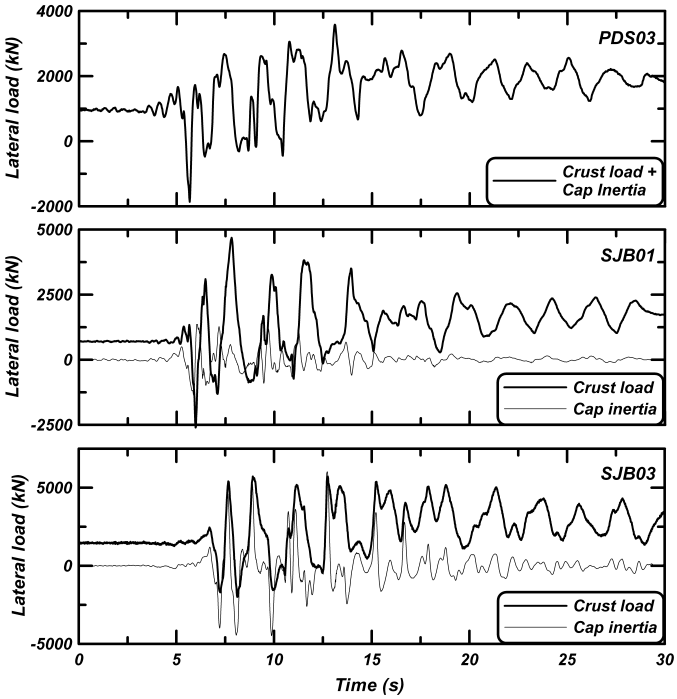


**Figure 8: Time series of the lateral crust loads imposed on the six-pile groups from PDS03, SJB01 and SJB03.**

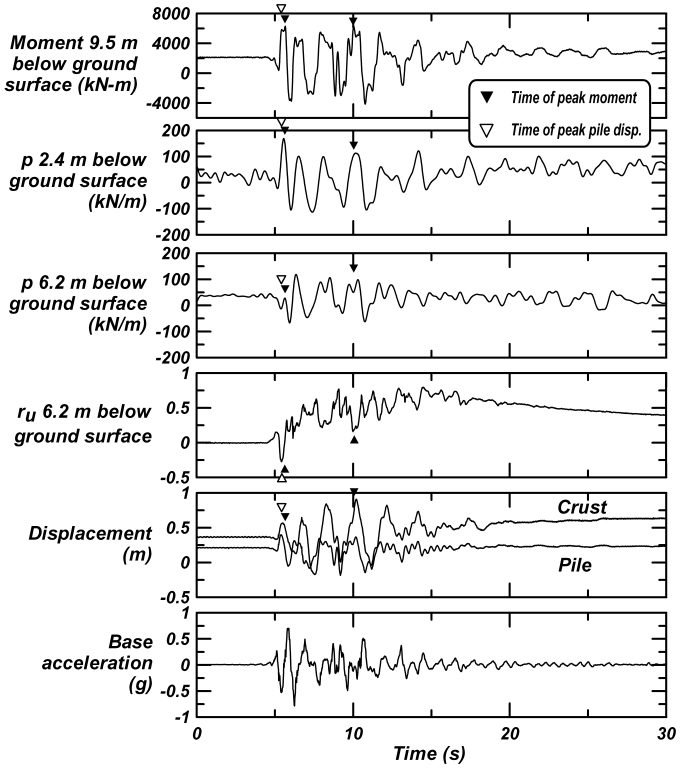


**Figure 9: Representative time series from PDS01 for the large-diameter single pile, BP, for a large Kobe motion.**

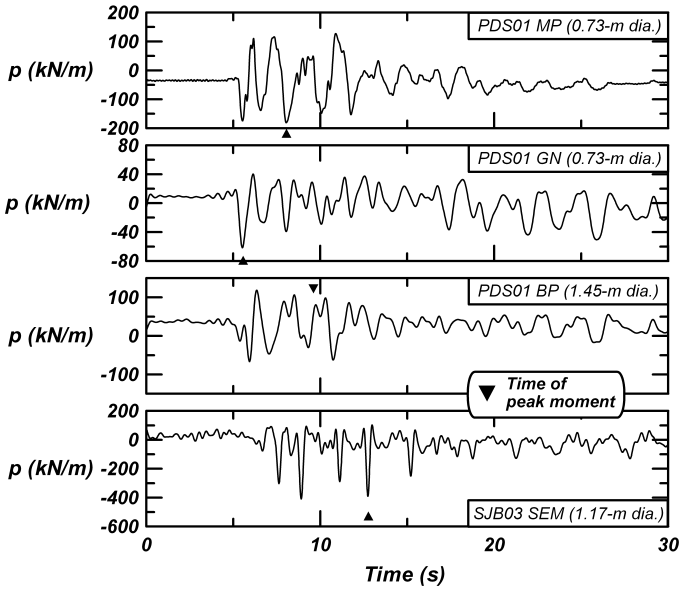


**Figure 10: p-histories near the middle of the loose sand for MP, GN and BP from PDS01 and SEM from SJB03 during a large Kobe motion.**

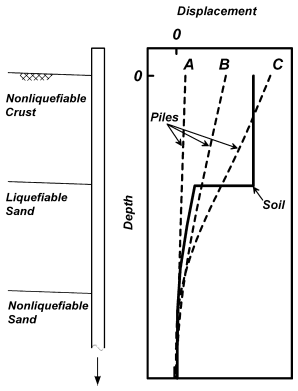


**Figure 11: Schematic of soil and pile displacements for cases where the piles (A) resisted the passive force of the crust with down-slope driving forces from the loose sand, (B) resisted the passive force of the crust with upslope resisting forces from the loose sand, and (C) were not stiff and/or strong enough to resist the down-slope passive force of the crust (C).**

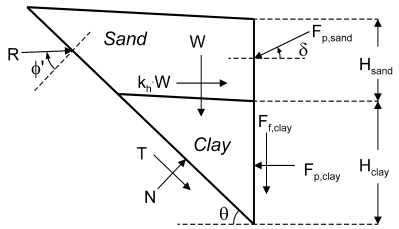


**Figure 12: Free-body diagram for a two-layer Coulomb-based passive force analysis.**

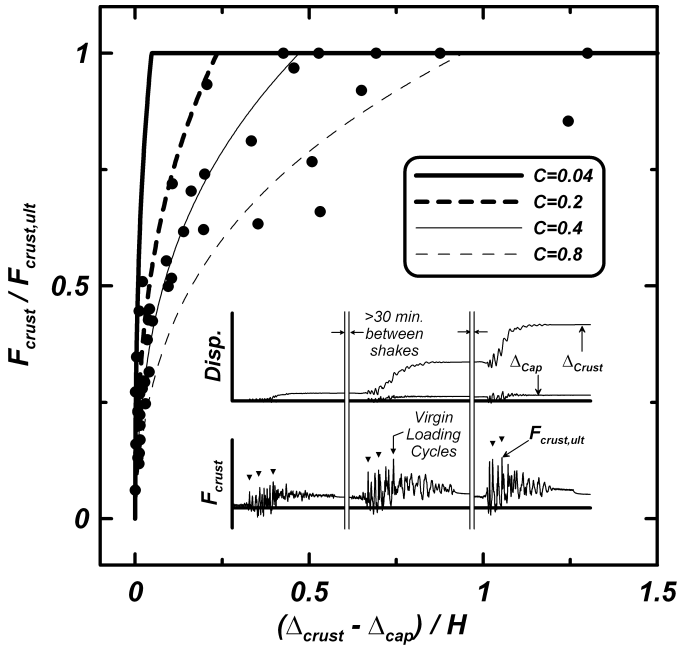


**Figure 13: Normalized load vs. normalized relative displacement from centrifuge tests and various trend lines calculated using Eq. (9).**

Table 1: Soil and pile properties for four of the centrifuge models.

| Test ID | Pile Foundation Properties[a] | Soil Profile | N[b] |
|---|---|---|---|
| PDS01 | Single pile: b=0.36 m[c]<br>Single pile: b=0.73 m[d]<br>Single pile: b=1.45 m[e]<br>Two-pile group: b=0.73 m[d] | 1.0 m Monterey sand<br>over 2.9 m clay ($s_u \approx$ 22 kPa)[f]<br>over 4.8 m loose sand ($D_r \approx$ 26%)<br>over dense sand ($D_r \approx$ 80%) | 38.1 g |
| PDS03 | Six-pile group (2x3): b=0.73 m[c]<br>Cap L,W,H=9.5 m, 5.7 m, 2.3 m | 4.2 m clay ($s_u \approx$ 22 kPa)[f]<br>over 4.6 m loose sand ($D_r \approx$ 31%)<br>over dense sand ($D_r \approx$ 79%) | 38.1 g |
| SJB01 | Six-pile group (2x3): b=0.73 m[c]<br>Cap L,W,H=10.1 m, 6.5 m, 2.5 m | 4.2 m clay ($s_u \approx$ 44 kPa)[f]<br>over 4.6 m loose sand ($D_r \approx$ 33%)<br>over dense sand ($D_r \approx$83%) | 38.1 g |
| SJB03 | Six-pile group (2x3): b=1.17 m[c]<br>Cap L,W,H=14.3 m, 9.2 m, 2.2 m | 1.4 m Monterey sand<br>over 2.7 m clay ($s_u \approx$ 44 kPa)[f]<br>over 5.4 m loose sand ($D_r \approx$ 35%)<br>over dense sand ($D_r \approx$ 75%) | 57.2 g |

[a] b = pile diameter, L = pile cap length, W = pile cap width, H = pile cap thickness
[b] N = Centrifugal acceleration
[c] E = 39 GPa; $\sigma_y$ = 38 MPa with nonlinear strain-hardening after yield; pile wall thickness, t = 34 mm.
[d] E = 68.9 GPa; $\sigma_y$ = 216 MPa; t = 34 mm at N = 38.1 g and t = 63 mm at N = 57.2 g.
[e] E = 68.9 GPa; $\sigma_y$ = 297 MPa; t = 63 mm.
[f] Average $s_u$ value over layer thickness.

Table 2: Summary of important quantities recorded at the time of the peak measured bending moment for each shake for centrifuge test SJB03.

| Motion | Bending Moment (kN·m)[a] | Crust Load (kN) | Pile Cap Inertia (kN) | p at 6.7 m depth (kN/m) [b] | $r_u$ at 6.7 m depth [b] | Pile Cap Displacement (m) | Crust Displacement (m) [c] |
|---|---|---|---|---|---|---|---|
| Small Santa Cruz | 1550 | 1560 | 1570 | -50 | 0.2 | 0.04 | 0.1 |
| Medium Santa Cruz | 3070 | 2870 | 1400 | -150 | 0.5 | 0.08 | 0.2 |
| Large Santa Cruz | 7080 | 6380 | 2560 | -310 | 0.7 | 0.3 | 1.3 |
| Large Kobe | 8840 | 5730 | 5790 | -370 | 0.5 | 0.5 | 2.3 |

[a] Bending moments were measured near the connection between the pile and the pile cap.
[b] Depth = 6.7 meters is near the center of the loose sand layer. $r_u$ values correspond to the transient dips at this instance in time, and were generally much greater immediately before and after.
[c] Crust displacement was measured at a location to the side of the pile cap.

Table 3: Summary of measurements from pile foundations in PDS01 for first large Kobe motion.

| Pile Foundation | Pile Diameter (m) | Peak Incremental Soil Surface Displacement (m)[a] | Peak Incremental Pile Displacement (m)[a] | Yielding of Pile | Peak Crust Load (kN)[b] | $p_l$ [c] (kN/m) |
|---|---|---|---|---|---|---|
| BP | 1.45 | 0.99 | 0.29 | None | 550 | 90 |
| GN | 0.73 | 0.55 | 0.48 | None | 280 | -60 |
| MP | 0.73 | 0.55 | 0.55 | None | 280 | -190 |
| SP | 0.36 | 0.99 | 1.29 | Extensive | n.a | n.a. |

[a] Displacements continued to accumulate through the earthquake sequence. Incremental displacements are relative to the displacements existing before each earthquake event.
[b] Estimated from p-histories at the middle of the clay layer, and extrapolated to boundaries using theoretical models for variation of p with depth.
[c] Subgrade reaction mobilized in middle of liquefied sand at time of peak moment.

Table 4: Estimated components of crust loads imposed on the pile groups.

| Test ID | Undrained Shear Strength, $s_u$ (kPa) | Adhesion Factor, $\alpha$ | Base Friction Reduction Factor, $R_{base}$[a] | Passive Force (kN) | Side Friction (kN) | Base Friction (kN) | Pile Segment Force (kN) | Total Crust Load (kN) | Peak Measured Crust Load (kN) |
|---|---|---|---|---|---|---|---|---|---|
| PDS03 | 22 | 0.6 | 0.5 | 1090 | 490 | 410 | 560 | 2550 | ≈2530[b] |
| SJB01 | 44 | 0.5 | 0.4 | 2320 | 950 | 700 | 1020 | 4990 | 4980 |
| SJB03 | 44 | 0.5 | 0.0 | 3500 | 450 | 0 | 2990 | 6940 | 6380 |
| DDC01[c] | 33 | 0.55 | 0.3 | 2600 | 650 | 680 | 2160 | 6090 | 6150[d] |
| DDC02[c] | 22 | 0.6 | 0.0 | 2090 | 480 | 170 | 1540 | 4280 | 4330[d] |

[a] Base friction force is defined as $\alpha \cdot R_{base} \cdot s_u \cdot A_{base}$

[b] Crust load is total measured load from the nonliquefied crust minus structural inertia load(s). Pile cap acceleration was not measured for PDS03, so the pile cap inertia was assumed equal to that measured in SJB01 at the time that the peak pile bending moments were recorded (approximately 620 kN).

[c] Pile cap dimensions were the same as for SJB03 (Table 1).

[d] An additional inertia force component from a single-degree-of-freedom superstructure attached to the pile cap was subtracted from the measured total shear to obtain crust load.

Table 5: Predicted and peak measured lateral crust loads on single piles.

| Pile | Peak measured p (kN/m) | Predicted $p_{ult}$ with static loading relations[a] (kN/m) | Predicted $p_{ult}$ with cyclic loading relations[a] (kN/m) |
|---|---|---|---|
| BP | 169 | 175 | 36 |
| GN | 82 | 90 | 22 |

[a] Using Matlock's (1970) p-y relations for static or cyclic loading as appropriate.